JCTC Journal of Chemical Theory and Computation

Computational ^{59}Co NMR Spectroscopy: Beyond Static Molecules†

Sonja Grigoleit and Michael Bühl*

Max-Planck Institut für Kohlenforschung, Kaiser-Wilhelm-Platz 1, D-45470 Mülheim an der Ruhr, Germany

Received October 12, 2004

Abstract: GIAO−B3LYP computations of ^{59}Co NMR chemical shifts are reported for $CoH(CO)_4$, $Co(CO)_4^-$, $CoCp(C_2H_4)_2$, $Co(CN)_6^{3-}$, $Co(NH_3)_3(CN)_3$, $Co(NH_3)_6^{3+}$, $Co(NH_3)_4(CO_3)^+$, $Co(acac)_3$, and $Co(H_2O)_6^{3+}$, employing both static calculations for equilibrium geometries as well as methods which include zero-point and classical thermal effects. The zero-point effects were computed by applying a perturbational approach, and the classical thermal effects were evaluated using Car-Parrinello molecular dynamics simulations. Both methods lead to a downfield shift of $\delta(^{59}Co)$ with respect to the equilibrium values, which can be attributed to a large extent to cobalt−ligand bond elongation. In some cases the zero-point and classical thermal corrections improve the agreement between computed and experimental values, but especially for complexes where the experimental NMR data were obtained in aqueous solution, the error increases somewhat. Mean absolute deviations between averaged and experimental $\delta(^{59}Co)$ values are on the order of 500−760 ppm over a chemical shift range of almost 20 000 ppm. The computed structures and properties of three $Co_2(CO)_8$ tautomers reproduce the experimental data very well. Two transition states for interconversion of these tautormers were located: low barriers are obtained, consistent with the observed fluxionality on the NMR time scale. Two model cobaloximes were taken as test cases to study the change of $\delta(^{59}Co)$ upon deuteration three bonds away from the metal. The sizable downfield shift of $\delta(^{59}Co)$ observed on going from H to D is attributed to a changed vibrational wave function, which causes a noticeable cobalt−ligand bond elongation.

Introduction

The ^{59}Co isotope had been prominent since the dawn of NMR spectroscopy, because it was one of the first nuclei for which the phenomenon of the chemical shift was observed.[1] To this day, the large chemical shift of this nucleus, on the order of 20 000 ppm,[2−4] together with rather favorable NMR properties, make ^{59}Co NMR spectroscopy a highly sensitive probe for the electronic structure, geometrical parameters, and reactivities of cobalt complexes.[5] In the surge of the blossoming life sciences, interest in ^{59}Co NMR of Co-containing biomolecules or model complexes thereof has recently been renewed.[6−9] Since the mid-1990s, the tools of density functional theory (DFT) have successfully been employed to calculate transition-metal chemical shifts,[10−13] and the ^{59}Co nucleus has been an early target for such computations.[14−17] In these studies, which confirmed the suitability of the B3LYP hybrid functional for chemical shift calculations of transition metals,[18] static computations were performed for optimized or experimental geometries. Current developments are directed to go beyond such a static picture in order to account for the dynamic nature of matter, thereby striving for an increase in the accuracy of theoretical NMR parameters. Methods that have been successfully applied to chemical shift calculations of lighter nuclei comprise solutions of the nuclear Schrödinger equations,[19] Quantum Monte Carlo Calculations,[20] perturbational zero-point corrections,[21−24] and molecular dynamics (MD) simulations.[25,26] The latter

* Corresponding author fax: (+49)208-306-2996; e-mail: buehl@mpi-muelheim.mpg.de.

† Dedicated to Prof. R. Ahlrichs on the occasion of his 65th birthday.

10.1021/ct049920o CCC: $30.25
Published on Web 01/13/2005

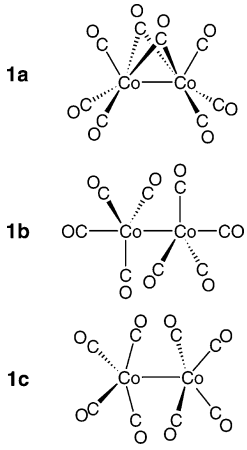

Figure 1. Tautomeric binuclear cobalt carbonyls.

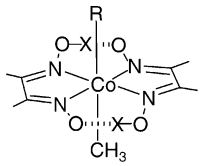

Figure 2. Cobaloximes of this study.

approach has also been used to evaluate solvent effects on transition-metal chemical shifts.[27−29]

In two recent studies[30,31] we have assessed the performance of the latter two methods, zero-point corrections and MD simulation, for a large number of Ti, V, Mn, and Fe complexes covering a total chemical shift range of ca. 4000 ppm. According to these systematic investigations, inclusion of zero-point and classical thermal effects does not lead to generally improved results but can afford more accurate δ(M) values in some cases. We now extend this systematic investigation to $\delta(^{59}\mathrm{Co})$ in order to test if the same conclusions are valid for this nucleus with its very large chemical shift range. For this purpose we have chosen a representative set of inorganic and organometallic cobalt complexes, which span almost 20 000 ppm in $\delta(^{59}\mathrm{Co})$, thereby increasing the range of chemical shifts covered so far by almost an order of magnitude. In addition to this systematic performance test, we report specific structural applications of ^{59}Co chemical shift calculations. The first of these applications concerns the dinuclear complex $Co_2(CO)_8$, a textbook example of a fluxional carbonyl complex, which exists in the form of at least two rapidly interconverting isomers in solution (see Figure 1). NMR spectra are thus observed as a dynamic average of the equilibrium mixture. If the isomers of this mixture would differ considerably in their $\delta(^{59}\mathrm{Co})$ values, sufficiently accurate computations of the latter could afford information on the relative isomer population.

The second application is related to an intriguing isotope effect in cobaloximes (see Figure 2). Asaro et al. have investigated ^{59}Co chemical shifts in cobaloximes [MeCo(Hdmg)$_2$py] (Hdmg = dimethylglyoximate, py = pyridine)[7] and found that the substitution of the two bridging hydrogen atoms by deuterium leads to a remarkably large change in $\delta(^{59}\mathrm{Co})$ ($\Delta\delta \approx 50$ ppm),[32] even though this substitution takes place three bonds away from the metal! This finding was rationalized in terms of a secondary geometrical effect, in which the fundamental vibrational wave function is modified, such that the mean r(O···D) distance becomes shorter than r(O···H), which, in turn, affects the r(O···O) distance and, ultimately the r(Co···N) bond length. For a deeper analysis of experimental results, we computed the vibrational averaged geometries and NMR chemical shifts of cobaloximes using the above-mentioned perturbational approach. Analysis of respective anharmonic contributions to the zero-point corrected geometries affords a deeper understanding of the geometrical effects on the ^{59}Co chemical shifts of cobaloximes. This case study of remote isotope effects is a stringent test for the perturbational zero-point corrections, a test which they are shown to pass.

Computational Methods

Geometries have been fully optimized employing the gradient-corrected exchange-correlation functionals of Becke[33] and Perdew,[34,35] denoted BP86, together with a fine integration grid (75 radial shells with 302 angular points per shell). For the optimization we employed basis AE1, that is, Wachters' all-electron basis augmented with one additional diffuse d and two p functions with the contraction scheme (14s11p6d)/[8s7p4d] for cobalt[36,37] and 6-31G* basis for all other elements. For the cobaloxime complexes we employed additionally basis AE1(*), that is, the same basis as AE1 and an additional p-polarization function on the two bridging hydrogen atoms. As shown before[31] the 6-31G* basis on the ligands is sufficient to compute molecular properties which depend on the curvature of the potential energy surface (PES). All structures were characterized as minima on the PES by the absence of imaginary harmonic vibrational frequencies or as transition states by the presence of exactly one imaginary frequency.

Magnetic shielding tensors have been computed with the gauge-including atomic orbitals method (GIAO) as implemented[38] in the Gaussian98 program,[39] employing the B3LYP hybrid functional[40,41] and Basis II′, that is, the same augmented Wachters basis set for cobalt and the IGLO−II basis[42] for the ligands except H: a (9s5p)/[5s4p] basis augmented with one set of d-polarization functions for C,N,O, and a (3s)/[2s] basis for H.

Molecular dynamics simulations were performed using the density-functional based Car-Parrinello scheme[43] as implemented in the CPMD program.[44] The BP86 functional was used, together with norm-conserving Troulier-Martins pseudopotentials in the Kleinman-Bylander form.[45,46]

Periodic boundary conditions were imposed by using supercells with box sizes between 10 and 14.5 Å so that the minimum distance between atoms in neighboring virtual boxes is larger than 6.3 Å. Kohn−Sham orbitals were expanded in plane waves up to a kinetic energy cutoff of 80 Ry. In the dynamic simulations a fictitious electronic mass of 600 au and a time step of 0.121 fs were used. From the microcanonical runs with an average temperature of 300 K snapshots were collected for the NMR calculations: after an equilibration time of 0.5 ps, 41 snapshots were taken every

Table 1: Equilibrium (r_e), Effective (r_{eff}), and Averaged (r_{av}) Geometrical Parameters for Co Complexes [in Å] BP86 Level[a]

			r_e(AE1)	r_{eff}	r_e(CP-opt)	r_{av}(CPMD)	exp
3	$CoH(CO)_4$	Co−H	1.495	1.503	1.496	1.500	1.556(18)[77]
		Co−C_{eq}	1.799	1.805	1.794	1.802	1.818(3)[77]
		Co−C_{ax}	1.804	1.809	1.805	1.817	1.764(10)[77]
		C−O_{eq}	1.163	1.154	1.154	1.156	1.141[77]
		C−O_{ax}	1.161	1.152	1.152	1.153	1.141[77]
4	$Co(CO)_4^-$	Co−C	1.777	1.782	1.771	1.777	1.735−1.769[78]
		C−O	1.183	1.180	1.175	1.176	1.132−1.172[78]
5	$CoCp(C_2H_4)_2$	Co−C(Cp)	2.107	2.116	2.109	2.126	
		Co−C(Et)	2.028	2.041	2.021	2.042	
6	$Co(CN)_6^{3-}$	Co−C	1.929	1.937	1.918	1.935	1.890[79]
		C−N	1.188	1.174	1.175	1.176	1.160[79]
7	$Co(NH_3)_3(CN)_3$	Co−N	2.070	2.087	2.077	2.113	
	(fac)	Co−C	1.851	1.856	1.844	1.851	
		C−N	1.184	1.181	1.172	1.173	
		N−H	1.029	1.018	1.027	1.030	
8	$Co(NH_3)_6^{3+}$	Co−N	2.032	2.047	2.019	2.045	1.972[79]
		N−H	1.036	1.021	1.032	1.035	0.980[79]
9	$Co(NH_3)_4(CO_3)^+$	Co−N_1	1.983	1.993	1.979	1.998	1.931(18)/1.953(14)[80]
		Co−N_2	2.042	2.057	2.033	2.051	2.031(22)[80]
		Co−O	1.892	1.900	1.920	1.921	1.905(11)[80]
		O−C	1.365	1.368	1.361	1.364	1.336(18)[80]
		N−H	1.032	1.017	1.028	1.032	
10	$Co(acac)_3$	Co−O	1.909	1.914	1.923	1.932	1.885/1.923[79]
11	$Co(H_2O)_6^{3+}$	Co−O	1.957	1.966	1.954	1.975	1.873(5)[81]
		O−H	0.995	0.984	0.990	0.993	

[a] For simplicity the averaged bond distance are given where appropriate.

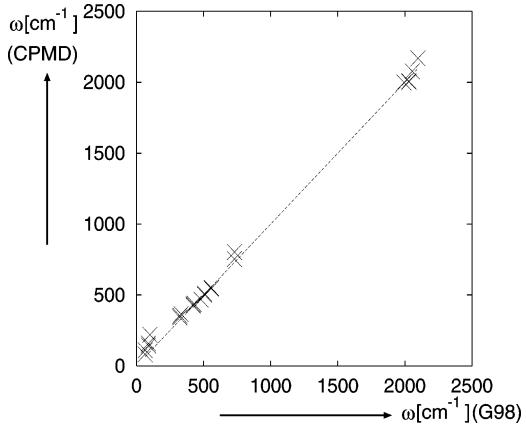

Figure 3. Harmonic frequencies of $CoH(CO)_4$ computed with G98 and CPMD to test the performance of the generated cobalt pseudopotential.

24 fs (total time ca. 1 ps). Equilibrium geometries for the compounds were obtained by optimizing the forces on all atoms with the CPMD program using the setup detailed above (denoted CP−Opt); additionally the averaged structural parameters were computed from the microcanonical run (denoted CPMD).

For cobalt no suitable pseudopotential was available; thus, a semicore potential was generated following the method described previously.[27,47] We used cutoff radii of 1.5 au for all three s-, p-, and d-channels. To test the performance of the generated pseudopotential we compared the computed optimized geometries of the test set in Figure 4 to those optimized using the above nonperiodic all-electron method.

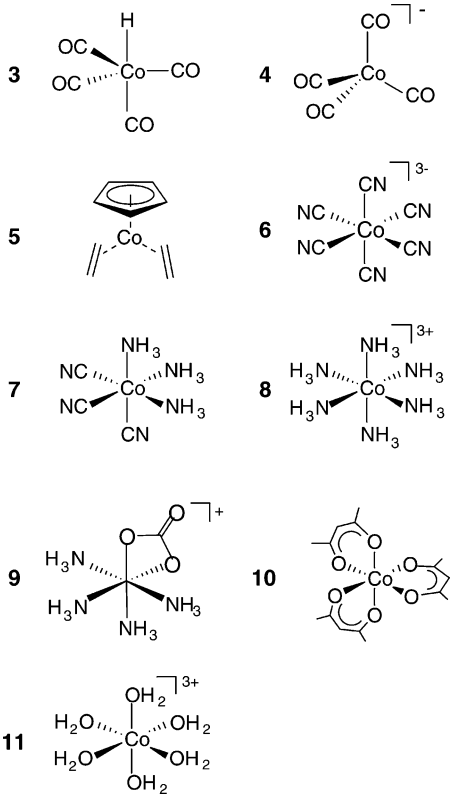

Figure 4. Co complexes of this study.

The bond lengths for both methods agree well within 1−2 pm (compare r_e(CP-opt) and r_e(AE1) data in Table 1). In addition, the vibrational frequencies of $CoH(CO)_4$ and

$Co(CN)_6^{3-}$ were computed. Judging from the slope of the regression line ($a = 0.99$) and the correlation coefficient ($r = 1.00$), the agreement of the harmonic frequencies computed with G98 and CPMD is exellent (Figure 3). Thus, the use of the generated pseudopotential (which is available from the authors upon request) seems to be well justified.

Vibrational corrections were computed using the perturbational approach of Ruud et al.[21−23] In this method, the molecule is first shifted from its equilibrium geometry r_e to an effective geometry r_{eff} via the harmonic frequencies ω_e and the cubic force field $V^{(3)}$:

$$r_{eff,j} = r_{e,j} - \frac{1}{4\omega_{e,j}^2}\sum_m \frac{V^{(3)}_{e,jmm}}{\omega_{e,m}} \quad (1)$$

This effective geometry corresponds to the vibrationally averaged structure of a system at 0 K.[48] Due to the anharmonicity of the PES the effective bond lengths are typically slightly longer than the equilibrium ones. Second, the magnetic shielding tensor is expanded in a Taylor series around this effective geometry. Thus, the expansion term containing the perturbed vibrational wave function to first order vanishes, and for the computation of the magnetic shielding to second order only the zeroth order vibrational wave function is needed. The equation for the calculation of the vibrationally averaged magnetic shielding is thus simplified to

$$\sigma_0 = \sigma_{eff} + \frac{1}{4}\sum_i \frac{\sigma^{(2)}_{eff,ii}}{\omega_{eff,i}} \quad (2)$$

where $\sigma^{(2)}_{eff}$ is the second derivative of the magnetic shielding, evaluated numerically, and σ_{eff} and ω_{eff} are magnetic shielding constant and the harmonic frequencies, both computed at the effective geometry.

In essence the vibrationally averaged magnetic shielding includes the leading contributions from both the anharmonicity of the PES (through the use of the effective geometry as an expansion point) and from the curvature of the magnetic shielding hypersurface.

For the computation of r_{eff} and σ_0 the corresponding parts of the Dalton program package[49] had been adapted so that energies, energy derivatives, and properties produced with Gaussian98 can be processed.[50] $V^{(3)}$ is obtained numerically at the BP86/AE1 level using the gradient technique, and a stepsize of 0.25 au for the finite displacements, as recommended by the test calculations in an earlier study.[50] For the computation of $\sigma^{(2)}_{eff}$ we used a stepsize of 0.1 au as recommended by the test calculations in the same study.[50]

To compute the effective geometries of $Co(NH_3)_6^{3+}$ with sufficient numerical precision, it was necessary to employ an ultrafine integration grid (99 radial shells with 590 angular points per shell). In this case the use of a smaller integration grid produces error-prone low-frequency modes of $-NH_3$ rotations which lead to abnormal, long N−H bond lengths (>1.3 Å). No such artifacts were encountered in the remaining molecules of the present study.

The magnetic shielding constants of the reference for relative δ values (aqueous $K_3[Co(CN)_6]$ in the experiment) have been evaluated by correlation of the computed shieldings σ(calc) of the complexes versus the experimental chemical shifts δ(exp) and by taking the respective axis intercepts of the linear regression lines as the estimated reference magnetic shielding for that particular level. Following this procedure we obtain σ_e(BP86/AE1) = −5837 ppm, σ_{eff} = −6060 ppm, σ_0 = −6124 ppm, σ_e(CP-opt) = −5753 ppm, and σ_{av}(CPMD) = −6203 ppm. Similar procedures had been adopted before in cases when a direct computation for the experimental standard is difficult or impossible.[18,51,52] As has been noted earlier,[14] these data are in good qualitative accord with experimental estimates for this absolute shielding value, around −5400 ppm.[53]

Results

Mononuclear Cobalt Complexes. The test set of mononuclear cobalt complexes is displayed in Figure 4. This set comprises electron-rich organometallic and high-valent inorganic Co(III) complexes and covers a chemical shift range of nearly 20 000 ppm.

The structural parameters of the equilibrium geometries, the zero-point corrected effective geometries, and the thermal averaged geometries of this test set are listed in Table 1. Where available, the corresponding experimental values are given. The computed bond lengths are in good accord with the experimental ones. The mean deviations from experiment are around 3.6 and 3.4 pm for the BP86/AE1 and CP-opt equilibrium geometries, respectively, where the computed bond lengths tend to be overestimated. This degree of agreement is typical for the type of density functional employed.[54] Both quantum-mechanical zero-point correction and classical thermal averaging lead to elongation of the cobalt−ligand bonds, thereby worsening the accord with experiment in comparison to the equilibrium values. The average Co−L bond elongation due to the zero-point effect is around 0.9 pm and due to thermal averaging 1.5 pm, leading to mean deviations from experiment of 3.8 and 4.0 pm, respectively (compare r_{eff} and r_{av} values with r_{exp} in Table 1). Similar results of bond elongation due to zero-point correction and thermal averaging were observed previously[31] for Ti, V, Mn, and Fe complexes.

An unusual effect is observed for the zero-point corrected structures. While all the cobalt−ligand bonds are elongated, the bonds between the ligand atoms coordinated directly to the metal center and an atom further away from the cobalt center are slightly contracted, on average by −0.9 pm (compare r_e(AE1) and r_{eff} in Table 1). The classical thermal effect, on the other side, leads to the expected bond elongation of intraligand bonds by an average amount of Δr = +0.2 pm (compare r_e(CP-opt) and r_{av} in Table 1). It is not clear at this point whether the extent of this unusual intraligand bond contraction is real or whether it is an artifact of the perturbational approach itself.

During the CPMD simulations of the cobalt complexes ligand rotations were observed. While the cyclopentadienyl ligand within the $CoCp(C_2H_4)_2$ complex rotates rather slowly (72° in 1.5 ps), the $-NH_3$, $-CH_3$, or $-OH_2$ groups within

Table 2: Equilibrium, Effective, Zero-Point Corrected, and Averaged Chemical Shifts in ppm of the Cobalt Complexes[d]

		δ_e(AE1)	δ_{eff}	δ_0	δ_e(CP-opt)	δ_{av}(CPMD)	exp
3	$CoH(CO)_4$	−3207	−3354	−3402	−3187	−3442	−3720[2]
4	$Co(CO)_4^-$	−2917	−3081	−3134	−2924	−3244	−3100[82]
5	$CoCp(C_2H_4)_2$	−1653	−1599	−1642	−1586	−1460	−1235[83]
6	$Co(CN)_6^{3-}$	576	586	546	272	477	0
7	$Co(NH_3)_3(CN)_3$	2994	3055	3019	2980	3260	3313[2]
8	$Co(NH_3)_6^{3+}$	9066	9596	9572	8537	9306	8176[2]
9	$Co(NH_3)_4(CO_3)^+$	8549	8834	8806	8703	9032	9700[84]
10	$Co(acac)_3$	11670	11770	-	12486	12686	12500[14]
11	$Co(H_2O)_6^{3+}$	16445	17344	17330	16493	18224	15100[85]
slope[a]		1.00	1.04[b]	1.08	1.02	1.08	
axis intercept[a]		94	95	89	44	78	
mean abs. dev.[c]		692	761	765	492	698	

[a] From a linear regression analysis with respect to the experimental value (using the estimated reference). [b] Without δ value of $Co(acac)_3$: 1.08. [c] Mean absolute deviation from experiment (using the estimated reference). [d] GIAO−B3LYP/II level, in parentheses: source of equilibrium, effective, or snapshot geometries.

$Co(NH_3)_3(CN)_3$, $Co(NH_3)_6^{3+}$, $Co(NH_3)_4(CO_3)^+$, $Co(acac)_3$, and $Co(H_2O)_6^{3+}$ rotate much faster, so that one or two complete turns occur during the simulation time of 1.5 ps. $Co(H_2O)_6^{3+}$ and $Co(NH_3)_6^{3+}$ are interesting in that respect because the minimum geometries display, due to small displacements of the ligands, symmetries which are lower than the highest possible ones. For the hexaquo complex, the preferred symmetry is S_6 instead of T_h, while for the hexammin complex it is C_3 instead of S_6. The respective energy differences between these forms are small, 6.5 and 1.6 kcal/mol for water and ammonia, respectively (BP86/AE1 level). Thus, interconversions via ligand rotations can occur readily in MD simulations at room temperature, and no specific symmetries can be assigned to the dynamically averaged structures.[55]

The chemical shifts of the cobalt centers computed at the equilibrium and the effective geometries as well as the zero-point corrected and thermally averaged chemical shifts are listed in Table 2. Since the experimental standard, aqueous $K_3[Co(CN)_6]$[2], is difficult to model computationally, we have evaluated the reference magnetic shielding from a correlation of theoretical σ versus experimental δ values (see computational details). The δ values for pristine $Co(CN)_6^{3-}$ are included in Table 2. The noticeable deviation from zero of these values indicates that, as expected, gaseous **6** is a poor model for the experimental standard and that solvent effects on this highly charged anion may be sizable.[56] For the isoelectronic $Fe(CN)_6^{4-}$, remarkably large solvent effects on the metal shielding constant, exeeding 1000 ppm, have been reported using suitable MD-based methods.[28] Similar simulations are in progress to model the aqueous solutions of Co complexes; the results of these demanding calculations will be reported in due course.

At the equilibrium geometries—computed both at BP86/AE1 and BP86/CP-opt levels, the chemical shifts tend to be shifted upfield with regard to the experimental values. The mean absolute error, 692 and 492 ppm, respectively, seems quite large at first sight. These errors, however, amount to but a few percent of the total ^{59}Co chemical shift range (ca. 19 000 ppm), a relative accuracy typical for DFT computed transition-metal chemical shifts so far.[12,13]

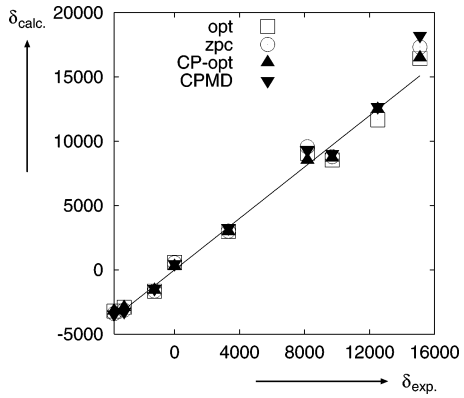

Figure 5. Plot of computed−GIAO−B3LYP for BP86/AE1 optimized (opt), zero-point corrected geometries (zpc), CP optimized (CP-opt), and thermally averaged geometries (CPMD)—versus experimental chemical shifts; solid line: ideal slope.

The slope of the δ_e(calc) versus δ(exp) regression lines are very close to the ideal value of 1 (see Table 2, Figure 5). Thus, our particular combination of DFT methods (B3LYP shifts for BP86 geometries) appears to perform very well in such static computations, without showing any signs of degradation at the deshielded end of the $\delta(^{59}Co)$ range.

Both zero-point correction as well as thermal averaging lead to a decrease of the shielding constants. Typically this downfield shift is larger in the substrates than that in the reference shieldings, resulting in an increase of the δ values. The two exceptions are $CoH(CO)_4$ and $Co(CO)_4^-$, where the downfield shifts are smaller than that of the reference, so that the overall effect is a decrease of δ. The mean absolute error increases somewhat upon zero-point correction and thermal averaging, namely from 692 to 765 and from 492 to 698 for δ_0 and δ_{av}, respectively. The larger slope of the corresponding regression lines (1.08 for the zero-point corrected and the thermal averaged chemical shifts, as compared to the near-ideal values for the corresponding δ_e data, see Table 2) also indicates that the zero-point corrected and thermal averaged chemical shift agree somewhat less perfectly with the experimental data than the chemical shifts at the equilibrium geometry.

Table 3: Shielding/Bond-Length Derivative $\partial\sigma_{Co}/\partial r_{Co-L}$ in ppm/pm of Cobalt Compounds[b]

			$\partial\sigma_{Co}/\partial r_{Co-L}$	"per bond"[a]
3	$CoH(CO)_4$	$Co-(CO)_4$	−118.0	−29.5
		Co−H	−23.4	−23.1
4	$Co(CO)_4^-$	$Co-(CO)_4$	−132.3	−33.1
5	$CoCp(C_2H_4)_2$	Co−Cp	−103.3	−103.3
		$Co-(C_2H_4)_2$	−113.2	−56.6
6	$Co(CN)_6^{3-}$	$Co-(CN)_6$	−311.9	−52.0
7	$Co(NH_3)_3(CN)_3$	$Co-(NH_3)_3$	−108.1	−36.0
		$Co-(CN)_3$	−245.4	−81.8
8	$Co(NH_3)_6^{3+}$	$Co-(NH_3)_6$	−471.1	−78.5
9	$Co(NH_3)_4(CO_3)^+$	$Co-(NH_3)_4$	−334.8	−83.7
		$Co-(CO_3)$	−109.6	−54.8
10	$Co(acac)_3$	$Co-(acac)_3$	−630.8	−105.1
11	$Co(H_2O)_6^{3+}$	$Co-(H_2O)_6$	−692.6	−115.4

[a] π-ligands counted as single ligand. [b] Explanation see text.

The largest offset due to zero-point correction and thermal averaging is obtained for $Co(H_2O)_6^{3+}$ and $Co(NH_3)_6^{3+}$, for which the experimental NMR shifts are obtained in aqueous solution. Together with $Co(CN)_6^{3-}$, these are the complexes with the largest overestimation of the cobalt−ligand bond lengths with respect to experiment (Table 1). It is well possible that also for these highly charged cations, interactions with a protic solvent (or polar surrounding) can affect geometries and NMR chemical shifts, as had been noted for highly charged anions.[28] The relatively good performance of the corresponding gas-phase equilibrium structures in the chemical shift calculations could then benefit to some extent from fortuitous error cancellation. Further investigations along this line are in progress.

As in our previous report,[31] we investigated the influence of the metal−ligand bond elongation on the NMR chemical shifts in a more quantitative manner. To this end, we have computed the metal shielding/bond-length derivatives employing the following procedure: the magnetic shielding constants σ have been computed at five different geometries, in which the bond length to each of symmetry-equivalent ligand atoms have been distorted from their equilibrium values by −1 pm to +3 pm while leaving all other parameters unchanged. The shielding/bond-length derivatives $\partial\sigma_{Co}/\partial r_{Co-L}$ have been determined by linear regression (see Table 3). Qualitatively we obtained similar results as for the Ti, V, Mn, and Fe complexes studied previously. The largest $\partial\sigma_{Co}/\partial r_{Co-L}$ values are attributed to the 6-π-ligand Cp and to the oxygen ligands, $-OH_2$ and (acac). For $Co(CN)_6^{3-}$, an experimental estimate is available for this quantity, based on isotope effects on the force field and the ^{59}Co chemical shift.[57] As has been noted before,[14] this experimental value,[57] $\partial\sigma_{Co}/\partial r_{Co-L} = -75$ ppm pm^{-1} is somewhat underestimated at the B3LYP level, cf. the value of −52 ppm pm^{-1} given in Table 3. As is the case for other transition-metal complexes,[31] the individual $\partial\sigma_{Co}/\partial r_{Co-L}$ increments for a given ligand L are not transferable between complexes but increase in absolute value with the deshielding of the metal. For instance, the $\partial\sigma_{Co}/\partial r_{Co-N}$ values of the ammonia ligands in $Co(NH_3)_3(CN)_3$ and $Co(NH_3)_6^{3+}$ are ca. −36 and −79 ppm, respectively (see per bond values in Table 3), paralleling the increase in $\delta(^{59}Co)$ in this series, from $\delta = 3313$ to 8176 ppm (Table 2). The shielding/bond-length derivatives are negative for all cobalt complexes in this study. However, this is not generally the case, for example when spin−orbit effects come to play they could be positive.[58,59]

To investigate to what extent the change in chemical shift due to zero-point correction and thermal averaging can be traced back to bond elongations, we have multiplied the elongation of each metal−ligand bond with the corresponding shielding/bond-length derivative and summed up all the products for each complex. The estimated differences $(\sigma_e - \sigma_{av})_{estd}$ and $(\sigma_e - \sigma_{eff})_{estd}$ are compared to the actual calculated difference in the magnetic shielding $(\sigma_e - \sigma_{av})_{calc}$ and $(\sigma_e - \sigma_{eff})_{calc}$in Table 4, and are plotted in Figure 6.

For the zero-point corrected chemical shifts, these estimated differences agree well with the calculated values, except for the $Co(H_2O)_6^{3+}$ complex. Judging from the slope of the regression line, the bond elongation accounts for 91% of the downfield shift due to zero-point correction (neglecting the $Co(H_2O)_6^{3+}$ values). It is unclear why the estimated difference $(\sigma_e - \sigma_{eff})_{estd}$ of the $Co(H_2O)_6^{3+}$ complex only covers approximately half of the value of the actual calculated difference $(\sigma_e - \sigma_{eff})_{calc}$ It is possible that in this case, the influence of bond angles on the chemical shift is larger than assumed.

For the thermally averaged chemical shifts, the estimated and calculated differences agree to a somewhat lesser extent. In this case the bond elongation accounts, on average, for 72% of the downfield shift. We obtained similar results for the complexes of Ti, V, Mn, and Fe in our previous report,[31]

Table 4: Difference between Thermally Averaged and Equilibrium Magnetic Shieldings $\sigma_e - \sigma_{av}$ and between Magnetic Shieldings at Effective and Equilibrium Geometry[a]

		$(\sigma_e - \sigma_{eff})_{estd}$	$(\sigma_e - \sigma_{eff})_{calc}$	$(\sigma_e - \sigma_{av})_{estd}$	$(\sigma_e - \sigma_{av})_{calc}$
3	$CoH(CO)_4$	89	76	115	195
4	$Co(CO)_4^-$	66	59	79	130
5	$CoCp(C_2H_4)_2$	262	277	321	576
6	$Co(CN)_6^{3-}$	250	233	530	655
7	$Co(NH_3)_3(CN)_3$	306	284	561	730
8	$Co(NH_3)_6^{3+}$	707	753	1225	1219
9	$Co(NH_3)_4(CO_3)^+$	484	508	427	779
10	$Co(acac)_3$	315	323	568	650
11	$Co(H_2O)_6^{3+}$	623	1122	1454	2181

[a] estd: estimated using the shielding/bond-length derivatives from Table 3 multiplied with the corresponding differences in bond lengths from Table 1 and calc: actual calculated differences from Table 2.

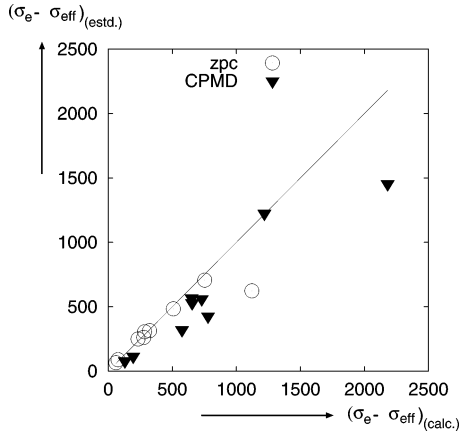

Figure 6. Plot of estimated vs calculated differences between effective and equilibrium magnetic shieldings $\sigma_e - \sigma_{eff}$ (zpc) and between thermally averaged and equilibrium magnetic shieldings $\sigma_e - \sigma_{av}$ (CPMD); data from Table 4; line: ideal slope.

Table 5: Computed (GIAO−B3LYP for BP86/AE1 Optimized Geometries) and Experimental Elements of the ^{59}Co Chemical Shielding Tensor (σ_{11}, σ_{22}, σ_{33})[c]

	σ_{ii}(opt)	σ_{ii}(eff)	σ_{ii}(CP-opt)	σ_{ii}(CPMD)	σ_{ii}(exp)
9	−875	−969	−871	−1210	−667[84]
	−220	−294	12	−174	−167
	1095	1262	859	1383	833
10	−449	−487	−538	−962	−686[a]
	220	231	231	20	212
	230	255	306	944	473
12	−672	−536			−696[b]
	211	176			232
	463	362			464

[a] $\delta_{iso} = 12505(1)$ ppm, $\Omega = 1159(46)$ ppm, $\kappa = -0.55(5)$.[4] [b] Exptl data for **2**, $\delta_{iso} = 3640(100)$ ppm, $\Omega = 1160(50)$ ppm, $\kappa = -0.6(2)$.[4] [c] Traceless representation.

where an average slope of 63% for the corresponding linear regression line has been obtained. Thus, we can also state for the cobalt complexes that it is indeed the metal−ligand bond distances that are most important for the chemical shift of the metal nucleus and its sensitivity toward temperature effects.[60] The remaining discrepancies between estimated and calculated effects on σ(Co) are probably due to nonadditivity of the increments and the neglect of L−Co−L bendings.

The Magnetic Shielding Tensor. In a number of cases, information on the full ^{59}Co magnetic shielding tensor is known from solid-state ^{59}Co NMR spectroscopy.[4] To investigate the influence of zero-point vibration and thermal averaging in more detail we have taken a look at individual shielding-tensor elements of three example compounds, namely of **9**, **10**, and **12**, a model for the cobaloxime **2** lacking the four peripheral methyl groups at the glyoximate ligands (see section on cobaloximes below). The other complexes of the present study were not included as either there were no shielding tensors reported in the literature or there were multiple sites in the NMR spectrum. The computed and experimental elements of the traceless shielding tensor (i.e. the values relative to the isotropic average) are listed in Table 5. The slopes of the σ_{ii}(calc) versus σ_{ii}(exp) regression lines are 1.03 and 0.97 at the BP86/AE1 and CP-optimized geometries, respectively, which is very close to the ideal slope of 1. The tensor elements at the effective geometry do not differ significantly from those at the static optimized geometry. The slope of the regression line is also quite similar with a value of 1.06. Also, there is no general trend in the change of the shielding tensor elements from the optimized to the effective geometry. For **9** the range of the values covered by the tensor elements is increased, while for **12** the range is reduced. The thermal averaged tensor elements agree significantly less with the experimental data (slope = 1.63). In general, the thermal averaging leads to a broadened span of the shielding tensor elements, and the deviation from the experimental values increases in the smallest and largest tensor elements. It is possible, that due to the thermal movement in the gas phase "extreme" geometries are obtained which lead to far higher (or lower) values in the tensor elements in comparison to those at the static optimized geometries. The experimental data, on the other hand, are taken from crystals or powder samples, where the thermal movement does not allow such "extreme" geometries.

Finally we have investigated the tensor of the electric field gradient (EFG). First, the largest component of the EFG tensor q_{zz} can be compared directly to experimental values from the nuclear quadrupole coupling constant, $e^2q_{zz}Q/h$ (Q: nuclear quadrupole moment). The computed q_{zz} values at the optimized geometry agree both in sequence as in order of magnitude with the experimental data (see Table 6).[61]

Table 6: Largest Component q_{zz} of the B3LYP/II′ Computed Electric Field Gradient at the ^{59}Co Nucleus in a.u., Square of q_{zz}, the Thermally Averaged q_{zz}, the Experimental q_{zz} Computed from the Nuclear Quadrupole Coupling Constant e$q_{zz}Q/h$ in MHz and the Experimental Line Widths in Hz

	at r_e(BP86/AE1)		CPMD		exp		
	$\lvert q_{zz}\rvert$	q_{zz}^2	$\lvert<q_{zz}>\rvert$	$<\lvert q_{zz}\rvert>$	$eq_{zz}Q/h$	q_{zz}	$\Delta\nu_{1/2}$
3	1.365	1.863	0.931	1.370	101−163[a]	1.023−1.652	3265[82]
5	1.833	3.360	1.925	1.925			6800[83]
6	0.000	0.000	0.041	0.371	6.2[2]	0.063	6 ± 1.5;[2] 202[86]
7	0.062	0.004	0.094	0.310			750 ± 50;[2] 1007[86]
8	0.011	0.000	0.079	0.367	0.97(1)−3.37(1)[2]	0.010−0.034	183 ± 10;[2] 202[86]
9	0.427	0.182	0.042	0.503	18.82(1)[2]	0.191	5476 ± 400[2]
10	0.022	0.000	0.003	0.235	5.53(7)[2]	0.056	
12	0.492	0.242			29.6(4)[2]	0.300	3100[87]

[a] For $XCo(CO)_4$ with X = $SiPh_3$ and X = $SnCl_3$.[2]

Table 7: Equilibrium (r_e) Geometrical Parameters in Å and Relative Energy (BP86/AE1) of **1a**−**1e**[a]

	r_e(Co−Co)	r_e(Co−C_a)	r_e(Co−C_b)	r_e(Co−C_c)	r_e(Co−C_d)	E [kJ/mol]
1a	2.550	1.809	1.820	1.958		0
exp[88] (**1a**)	*2.528(1)*	*1.815(1)*	*1.832(4)*	*1.939(4)*		
1b	2.697	1.812	1.775			27.0
1c	2.633	1.797	1.803			16.7
1d (**1b** → **1c**)	2.694	1.798	1.804	1.776	1.832	36.1
1e (**1c** → **1a**)	2.613	1.808	1.801	1.807	1.802	18.6

[a] See Figure 7 for numbering of atoms.

When analyzing the thermally averaged q_{zz} values, we should distinguish between highly symmetric molecules, which have tensor elements of approximately zero at the optimized geometry and unsymmetric molecules with high q_{zz} values. In the first case, we notice a strong oscillation of q_{zz} around zero, whereas the average value $| < q_{zz} > |$ is very small (<0.08). The unsymmetric molecules, on the other hand, oscillate around the respective q_{zz} value at the optimized geometry (e.g. for **3** the value oscillates between | 1.1| and | 1.8|), so that the average absolute value is only slightly larger than the q_{zz} value at the static geometry (1.370 instead of 1.365 at the optimized geometry).

We also attempted to correlate the intense line broadening which is caused by the interaction of the quadropole moment of the ^{59}Co nucleus (I=7/2) with the EFG at the nucleus. However, we did not obtain a meaningful correlation between q_{zz} (either computed or taken from nuclear quadrupole resonance spectroscopy) and the experimental line width, $\Delta\nu_{1/2}$, which for a quadropole relaxation is expected to be[62]

$$\Delta\nu_{1/2} \propto q_{zz}^2(1 + \eta^2/3)\tau_c \qquad (3)$$

(η: asymmetry parameter of the EFG tensor, τ_c: molecular correlation time). The main reason is probably that the line width also depends on other factors such as temperature, solvent or molecular size, and the EFG need not always be decisive. Similar findings have been reported for other nuclei such as ^{99}Ru[51] and ^{49}Ti.[30]

Dicobalt Octacarbonyl

Dicobalt octacarbonyl is not included in the test set discussed so far, because its structure in solution is fluxional. For instance only one signal is found in the ^{13}C NMR spectrum.[63] Doubly bridged **1a** is found in the crystal,[64] but other forms such as **1b** and **1c** have been proposed in matrix-isolation studies.[65] Earlier DFT studies have confirmed that **1a**−**1c** are quite similar in energy, but the relative stabilities can vary with the particular functional employed.[66,67] If the chemical shift of the individual isomers would be sufficiently different from each other, comparison of computed and experimental δ values could afford new evidence concerning the equilibrium mixtured in the NMR experiment. Similar structural applications of chemical shift calculations have been reported before.[12,68] In addition to the minima **1a**−**1c**, we have also located transition structures connecting them, which—to our knowledge—have not been reported yet.

The optimized geometrical parameters of stable cobalt carbonyls as well as those of the transition states are listed in Table 7. The computed values of **1a** agree very well with the experimental values of the crystal structure; the computed and experimental bond length agree better than 1%. Kenny et al. reported about similar good values using the BP86 density functional and a double-ζ plus polarization basis.[66] Energetically the C_{2v} symmetric **1a** is the most stable structure—**1b** and **1c** lie higher in energy by 27.0 and 16.7 kJ/mol, respectively, very close to the corresponding values of 26.4 and 15.5 kJ/mol obtained by Kenny et al.[66]

Table 8: Chemical Shifts[89] of **1a**−**1e**[a]

	Co	C_a	C_b	C_c	C_d	$C_{average}$
1a	−2265	186.8	197.0	233.5		203.6
1b	−2399	193.7	217.0			199.5
1c	−2354	208.7	198.8			203.8
1d (**1b** → **1c**)	−2326	203.2	200.3	213.4	187.1	201.1
1e (**1c** → **1a**)	−2282	194.7	201.3	204.7	211.5	203.1
exp	*−2200*[71]					*203.2*[63]

[a] See Figure 7 for numbering of atoms; GIAO−B3LYP/II level.

We have located 2 different transition states (**1d** and **1e**), one between **1b** and **1c** and one between **1a** and **1c**. Despite considerable effort, we could not locate a transition state connecting **1a** and **1b**. Even in the absence of the latter, interconversion between the two isomers **1a** and **1b** is possible via isomer **1c**. Both transition states were identified by a single imaginary vibrational frequency each, which describes the movement of transformation between the two minima they connect. Additionally, each transition state was checked by following the intrinsic reaction coordinate (IRC)[69,70] from the transition state to the two reactants. The two transition states are C_2-symmetric, i.e. one C_2 axis is preserved during the transitions $D_{3d} \rightarrow D_{2d}$ and $C_{2v} \rightarrow D_{2d}$. The Co−Co bond length of the transition states is of a similar value as in the unbridged structures **1b** and **1c**. Energetically these transiton states do not lie much higher than the reactants. The largest energy difference (between **1a** and **1d**) amounts to 36 kJ/mol (see Table 7). Thus, the interconversion of all three isomers should readily take place at a reasonable rate at room temperature. These results are fully consistent with the observed fluxionality on the NMR time scale.

Our computed NMR chemical shifts show that the δ(^{59}Co) values of **1a**−**1c** lie close together (see Table 8), between −2265 ppm and −2399 ppm, and agree well with the experimental value of −2200 ppm.[71] The differences between the chemical shifts of **1a**−**1c** are much smaller than the mean absolute errors in the computed δ(^{59}Co) values (Table 2). Thus, no structural assignments can be made on the basis of the δ(^{59}Co) values. Likewise, the computed ^{13}C chemical shifts do not appear to be of diagnostic value for

the structure in solution. While in the static structures, the chemical shifts of terminal C−O groups (between 186 and 217 ppm) could be discriminated from those of a bridging carbonyl group (234 ppm in **1a**), the $\delta(^{13}C)$ value averaged over all C atoms of a given isomer (which should be compared to the single, dynamic average observed in solution) shows only fairly little variation between **1a** and **1c**.

As the average Co−C bond length in structure **1a** is 5 pm longer than in **1b** and **1c**, we would expect a shift to higher fields for **1b** and **1c**. As this is not the case, it is very probable that the low field shift is due to the increase in the Co−Co bond length from **1a** to **1b** and **1c**. Using the computed shielding/bond-length derivative for the Co−Co bond of **1b** (-11.6 ppm pm^{-1}), we obtain an estimated value $\Delta\delta(^{59}Co) = 171$ ppm for **1b** and $\Delta\delta(^{59}Co) = 96$ ppm for **1c**, which resembles the calculated values of 134 and 89 ppm, respectively.

The computed vibrational harmonic frequencies of **1a** to **1c** agree very well with the data of Kenny et al.,[66] obtained at a similar level, and with experiment, where available. We provide these data as Supporting Information and refrain from a deeper discussion.

Cobaloximes

Cobaloximes are important model complexes for cobalamines and vitamin B_{12}.[72] Consequently, a sizable amount of spectroscopical data, including $\delta(^{59}Co)$ values are available.[2,6,73] Here we pay special attention to the effect of deuteration of a remote H-bond on the $\delta(^{59}Co)$ chemical shift, as observed in the dimethylglyoximato complex ([MeCo(Hdmg)$_2$py][7] (Hdmg = dimethylglyoximate, py = pyridine, **2**). We have considered two smaller model systems, **12** and **13**, with glyoximato ligands (i.e. lacking the four methyl groups at the periphery) and pyridine (**12**) or imine $H_2C{=}NH$ (**13**) as a model for the latter. The deuterated compounds in which H_{10} and H_{11} (see Figure 8) are substituted by deuterium are labeled as **12a** and **13a**, respectively. Changing an isotope within a molecule has no effect on the equilibrium geometry but alters the vibrational wave function of the molecule. Thus, the effect of deuteration has to be investigated by including the anharmonic vibrations and computing the vibrationally averaged geometry. Secondary isotope effects (i.e. by changing an isotope next to the resonating nucleus) have been reproduced with a variety of approaches.[24] An isotope effect over three bonds, however, as in **2**, is a much more challenging task. We have computed the zero-point corrected effective geometries using the same perturbational approach as discussed above and computed the NMR chemical shift δ_{eff} at these effective geometries. We have not computed the fully zero-point corrected value, δ_0, as the differences between δ_0 and δ_{eff} tend to be very small (see Table 2) and do not warrant the extra effort that would be necessary to evaluate δ_0 for a system as large as **12**. In Table 9 the BP86/AE1 and BP86/AE1(*) optimized geometries as well as the effective geometries of **12**, **12a**, **13**, and **13a** are listed.

On going from the equilibrium to the effective geometry of **13**, the bridging proton is shifted toward a more symmetric position between the two oxygen atoms, as evidenced by the change in the O−H/H···O distances from 1.09/1.43 Å (r_e) to 1.18/1.27 Å (r_{eff}, Table 9). Upon deuteration, the hydrogen atom is shifted back from this more mid-positioned site between the two oxygen atoms to a more asymmetric position close to one of the oxygen atoms but not as asymmetric as in the equilibrium structure (cf. the O−H/H···O distances of 1.15/1.32 Å for **13a** in Table 9). This finding is consistent with a potential energy surface which forms a double well along the O···H−O path with a low central barrier and a pronounced anharmonicity.[74] We have located the transition state for migration of the hydrogen between the two oxygen atoms in **13**, (O···H−O) ↔ (O···H···O) ↔ (O−H···O). The transition state is nearly C_s-symmetric except for the methyl group, which is rotated out of the symmetry plane, and shows a more mid-positioned

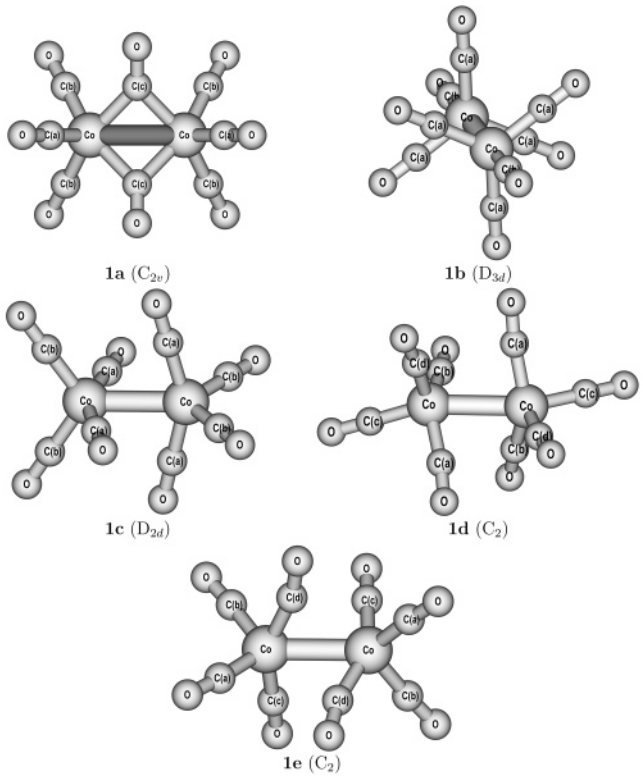

Figure 7. BP86/AE1 optimized geometries of $Co_2(CO)_8$ isomers (**1a**−**1c**) and transition states (**1d** and **1e**).

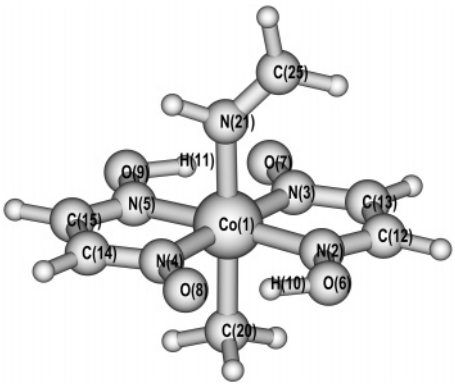

Figure 8. BP86/AE1(*) optimized geometry of **2a**.

Table 9: Equilibrium (r_e) and Effective (r_{eff}) Geometrical Parameters in Å of **12** and **13**[c]

	atoms	r_e (**12**)[a]	r_{eff} (**12**)[a]	r_{eff}(D) (**12a**)[a]	r_e (**13**)[b]	r_{eff} (**13**)[b]	r_{eff}(D) (**13a**)[b]
Co−N	1−2	1.898	1.903	1.903	1.892	1.899	1.900
	1−3	1.922	1.918	1.921	1.912	1.905	1.911
	1−4	1.922	1.919	1.922	1.920	1.913	1.918
	1−5	1.897	1.902	1.902	1.901	1.907	1.907
Co−Imin	1−21	2.069	2.083	2.084	1.980	1.995	1.996
Co-Me	1−20	2.012	2.026	2.025	2.009	2.021	2.020
O − H,D	6−10	1.066	1.122	1.104	1.085	1.180	1.149
	8−10	1.497	1.393	1.428	1.430	1.278	1.331
	7−11	1.484	1.381	1.418	1.420	1.262	1.317
	9−11	1.068	1.127	1.108	1.089	1.188	1.156
O ···O	6−8	2.551	2.506	2.522	2.506	2.452	2.473
	7−9	2.540	2.499	2.515	2.499	2.444	2.465

[a] AE1 basis. [b] AE1(*) basis. [c] BP86 level; see Figure 8 for numbering of atoms.

Table 10: Equilibrium (δ_e) and Effective (δ_{eff}) ^{59}Co Chemical Shifts in ppm (GAIO−B3LYP/II Level) of **12** and **13**

	basis[a]	δ_e	δ_{eff}
12	AE1	3362	3211
12a	AE1	3362	3276
13	AE1	3120	2977
13	AE1(*)	2943	2761
13a	AE1	3120	3043
13a	AE1(*)	2943	2847
2 *exp*[b]			*≈3640*
2a *exp*[b]			*≈3700*

[a] Used in energy evaluations together with BP86 functional. [b] Estimated from the spectrum plotted in ref 7, cf. footnote 32.

site of the migrating H atoms between the O-termini (r_e = 1.27/1.19 Å). This transition state is only 2.4 kJ/mol higher in energy than the ground state, so that the hydrogen can readily exchange between the two oxygen atoms at room temperature. Due to the dependence of the vibrational energy on the nuclear mass ($E \propto 1/\sqrt{m}$), the vibrational levels of the deuterated compound lie "deeper" inside the anharmonic potential well, so that in the vibrationally averaged geometry the deuterium is located closer to one of the two oxygen atoms. Similar findings have been reported for hydrogen bond model complexes (e.g., ClH:NH_3[75,76]).

The computed ^{59}Co chemical shifts of **12**, **12a**, **13**, and **13a** are summarized in Table 10. Employing Basis AE1 we compute an isotope effect $\Delta\delta = \delta_{eff}(Co,D) - \delta_{eff}(Co,H)$ of $\Delta\delta$ = 65 ppm for **12** and $\Delta\delta$ = 66 ppm for **13**. Employing Basis AE1(*), $\Delta\delta$ = 86 ppm is obtained for compound **13**, in very good agreement with the experimental value of $\Delta\delta \approx 50$ ppm.[7] Thus, both sign and magnitude of $\Delta\delta$ are correctly reproduced by the perturbational approach, which thus offers a faithful qualitative description of this effect.

Upon going from H to D, the main change in the coordination geometry about Co is found for the Co−N distances to the glyoximato ligands, which increase on average by 0.003 Å (Table 9). If we suppose that the corresponding shift in $\delta(^{59}Co)$ is based only on the increase of the Co−N bond length, then we can arrive at an estimated shielding/bond-length derivative of ≈72 ppm pm^{-1} per bond (using the $\Delta\delta$ value of **13** with AE1(*) basis). This value lies within the typical range of $\partial\sigma_{Co}/\partial r_{Co-N}$ derivatives (36−84 ppm/pm, see Table 3). Thus, the shift of $\delta(^{59}Co)$ due to the substitution of hydrogen by deuterium 3 atoms away from the metal center can by explained by an increase in the cobalt−ligand bond length due to a modified vibrational wave function, as anticipated during analysis of the experimental data.[7] According to our results, however, the extent of this bond elongation, well below 1 pm, is much less than estimated before.[7]

As a further test of the performance of the perturbational approach, we investigated the primary isotope effect, $^p\Delta = \delta(H) - \delta(D)$. Our computed values of $^p\Delta = +0.57$ ppm for **12**, Basis AE1 and $^p\Delta = +0.49$ ppm for **13**, Basis AE(*) agree very well with the experimental value of +0.38 ppm.[7] Thus, the task to reproduce such a small effect both in sign as well as in magnitude has been successfully accomplished.

Conclusions

We have applied different DFT-based methods to investigate the $\delta(^{59}Co)$ chemical shifts of a set of cobalt complexes that span nearly the entire chemical shift range of this nucleus. For this purpose we have performed static NMR chemical shift calculations at optimized geometries as well as computations which include zero-point or classical thermal effects. Overall, zero-point effects and thermal averaging result in a deshielding of ^{59}Co nuclei and also in an increase of most $\delta(^{59}Co)$ values. To a large extent these downfield shifts can be rationalized in terms of the bond elongation of the cobalt−ligand bonds. However, it is only in some cases that zero-point or thermally averaged chemical shifts are improved over the respective static equilibrium values. In general, the mean absolute error of the computed chemical shifts increases slightly, by 70 to 200 ppm, upon inclusion of zero-point or thermal effects, where the largest errors are observed mainly for those complexes that were measured in aqueous solution. In these cases, solvation effects are expected to be substantial, effects which will be addressed in future work.

In addition, we have investigated three tautomeric forms of the binuclear cobalt octacarbonyl and have located, for the first time, salient transition states connecting these minima. These transition states are computed ca. 2 to 36

kJ/mol above any of the tautomers, consistent with the fluxionality of this molecule on the NMR time scale. The $\delta(^{59}\text{Co})$ chemical shifts differ only slightly between the tautomeric forms and fall in a short-range less than 200 ppm, thereby preventing conclusions concerning the composition of the equilibrium mixture.

As further cobalt compounds we have investigated model cobaloximes, paying special attention to the effect of deuteration 3 bonds away from the metal center. Due to the changes in the vibrational wave function, the structure of the (O···H−O)-system is altered, such that the O−D bond is 3 pm shorter than the former O−H bond. This in turn leads to a slightly larger Co−N bond separation, which causes a considerable downfield shift of the cobalt center. Both sign and magnitude of this isotope effect, $\Delta\delta(^{59}\text{Co})$, agrees well with the experimental values.

Quantitative predictions of ^{59}Co chemical shifts, and those of transition metals in general, remain a challenge for approximate density functional theory, and the applied methods to include zero-point and classical thermal effects are no panacea and need further improvement, such as the inclusion of solvation effects. Nevertheless, the possibility to go beyond static molecules in ^{59}Co chemical shift calculations can open new possibilities for applications of such computations, thus affording an ever more refined theoretical complement to experimental ^{59}Co NMR spectroscopy.

Supporting Information Available: Harmonic vibrational frequencies at BP86/AE1 level of **1a**−**1c** (Table S1) and plot of computed - GIAO-B3LYP for BP86/AE1 optimized geometries - versus experimental elements of the chemical shielding tensor (Figure S1). This material is available free of charge via the Internet at http://pubs.acs.org.

References

(1) Proctor, W. G.; Yu, F. C. *Phys. Rev.* **1951**, *81*, 20.

(2) Pregosin, P. S. In *Transition Metal Nuclear Magnetic Resonance*; Pregosin, P. S., Ed.; Elsevier: Amsterdam, 1991; p 144.

(3) Yamasaki, A. *J. Coord. Chem.* **1991**, *24*, 211.

(4) Chan, J. C. C.; Au-Yeung, S. C. F. *Ann. Rep. NMR Spectrosc.* **2000**, *41*, 1.

(5) von Philipsborn, W. *Chem. Soc. Rev.* **1999**, *28*, 95.

(6) Medek, A.; Frydman, V.; Frydman, L. *Proc. Natl. Acad. Sci. U.S.A.* **1997**, *94*, 14237.

(7) Asaro, F.; Liguori, L.; Pellizer, G. *Angew. Chem., Int. Ed.* **2000**, *39*, 1932.

(8) Medek, A.; Frydman, L. *J. Am. Chem. Soc.* **2000**, *122*, 684.

(9) Pellizer, G.; Asaro, F.; Pergolese, B. *Magn. Reson. Chem.* **2004**, *42*, 756.

(10) Kaupp, M.; Malkin, V. G.; Malkina, O. L. In *Encyclopedia of Computational Chemistry*; Schleyer, P. v. R., Allinger, N. L., Kollman, P. A., Clark, T., Schaefer, H. F., Gasteiger, J., Schreiner, P. R., Eds.; Wiley: Chichester, 1998; Vol. 3, p 1857.

(11) Schreckenbach, G.; Ziegler, T. *Theor. Chem. Acc.* **1998**, *99*, 71.

(12) Bühl, M. In *Calculation of NMR and EPR Parameters. Theory and Applications*; Kaupp, M., Bühl, M., Malkin, V. G., Eds.; Wiley-VCH: Weinheim, 2004; p 421.

(13) Bühl, M.; Kaupp, M.; Malkin, M.; Malkina, V. G. *J. Comput. Chem.* **1999**, *20*, 91.

(14) Godbout, N.; Oldfield, E. *J. Am. Chem. Soc.* **1997**, *119*, 8065.

(15) Chan, J. C. C.; Au-Yeung, S. C. F.; Wilson, P. J.; Webb, G. A. *J. Mol. Struct. (THEOCHEM)* **1996**, *365*, 125.

(16) Chan, J. C. C.; Au-Yeung, S. C. F. *J. Mol. Struct. (THEOCHEM)* **1997**, *393*, 93.

(17) Chan, J. C. C.; Au-Yeung, S. C. F. *J. Phys. Chem.* **1997**, *101*, 3637.

(18) Bühl, M. *Chem. Phys. Lett.* **1997**, *267*, 251.

(19) Sundholm, D.; Gauss, J.; Schäfer, A. *J. Chem. Phys.* **1996**, *105*, 11051.

(20) Böhm, M. C.; Schulte, J.; Ramirez, R. *Int. J. Quantum Chem.* **2002**, *86*, 28.

(21) Ruud, K.; Åstrand, P.-O.; Taylor, P. R. *J. Chem. Phys.* **2000**, *112*, 2668.

(22) Ruud, K.; Åstrand, P.-O.; Taylor, P. R. *J. Am. Chem. Soc.* **2001**, *123*, 4826.

(23) Ruden, T.; Lutnæes, O. B.; Helgaker, T. *J. Chem. Phys.* **2003**, *118*, 9572.

(24) Ruden, T. A.; Ruud, K. In *Calculation of NMR and EPR Parameters: Theory and Applications*; Kaupp, M., Bühl, M., Malkin, V. G., Eds.; Wiley-VCH: Weinheim, 2004; p 153.

(25) Malkin, V. G.; Malkina, O. L.; Steinebrunner, G.; Huber, H. *Chem. Eur. J.* **1996**, *2*, 452.

(26) Searles, R. D. I.; Huber, H. In *Calculation of NMR and EPR Parameters. Theory and Applications*; Kaupp, M., Bühl, M., Malkin, V. G., Eds.; Wiley-VCH: Weinheim, 2004; p 175.

(27) Bühl, M.; Parrinello, M. *Chem. Eur. J.* **2001**, *7*, 4487.

(28) Bühl, M.; Mauschick, F. T. *Phys. Chem. Chem. Phys.* **2002**, *4*, 5508.

(29) Bühl, M.; Schurhammer, R.; Imhof, P. *J. Am. Chem. Soc.* **2004**, *126*, 3310.

(30) Bühl, M.; Mauschick, F. T. *Magn. Reson. Chem.* **2004**, *42*, 737.

(31) Grigoleit, S.; Bühl, M. *Chem. Eur. J.* **2004**, *10*, 5541.

(32) The value for single H/D substitution is given in ref 7 as $\Delta\delta = 25$ ppm; in the plotted spectrum, $\Delta\delta \approx 55$ ppm can be estimated for double substitution.

(33) Becke, A. D. *Phys. Rev. A* **1988**, *38*, 3098.

(34) Perdew, J. P. *Phys. Rev. B* **1986**, *33*, 8822.

(35) Perdew, J. P. *Phys. Rev. B* **1986**, *34*, 7406.

(36) Wachters, A. J. H. *J. Chem. Phys.* **1970**, *52*, 1033.

(37) Hay, P. J. *J. Chem. Phys.* **1977**, *66*, 4377.

(38) Cheeseman, J. R.; Trucks, G. W.; Keith, T. A.; Frisch, M. J. *J. Chem. Phys.* **1996**, *104*, 5497.

(39) Gaussian98 (revision A.7). Frisch, M. J.; Trucks, G. W.; Schlegel, H. B.; Scuseria, G. E.; Robb, M. A.; Cheeseman, J. R.; Zakrzewski, V. G.; Montgomery, J. A.; Stratman, R.

E.; Burant, J. C.; Dapprich, S.; Milliam, J. M.; Daniels, A. D.; Kudin, K. N.; Strain, M. C.; Farkas, O.; Tomasi, J.; Barone, V.; Cossi, M.; Cammi, R.; Mennucci, B.; Pomelli, C.; Adamo, C.; Clifford, S.; Ochterski, J.; Petersson, G. A.; Ayala, P. Y.; Cui, Q.; Morokuma, K.; Malick, D. K.; Rabuck, A. D.; Raghavachari, K.; Foresman, J. B.; Cioslowski, J.; Ortiz, J. V.; Baboul, A. G.; Stefanov, B. B.; Liu, C.; Liashenko, A.; Piskorz, P.; Komaromi, I.; Gomperts, R.; Martin, R. L.; Fox, D. J.; Keith, T.; Al-Laham, M. A.; Peng, C. Y.; Nanayakkara, A.; Gonzalez, C.; Challacombe, M.; Gill, P. M. W.; Chen, B. G. J. W.; Wong, M. W.; Andres, J. L.; Head-Gordon, M.; Replogle, E. S.; Pople, J. A. Gaussian, Inc., Pittsburgh, PA, 1998.

(40) Becke, A. D. *J. Chem. Phys.* **1993**, *98*, 5648.

(41) Lee, C.; Yang, W.; Parr, R. G. *Phys. Rev. B* **1988**, *37*, 785.

(42) Kutzelnigg, W.; Fleischer, U.; Schindler, M. *NMR: Basic Principles and Progress;* 1990; Vol. 23, p 165.

(43) Car, R.; Parrinello, P. *Phys. Rev. Lett.* **1985**, *55*, 2471.

(44) CPMD Version 3.3a. Hutter, J.; Alavi, A.; Deutsch, T.; Bernasconi, M.; Goedecker, S.; Marx, D.; Tuckermann, M.; Parrinello, M. Max-Planck-Institut für Festkörperforschung (Stuttgart) and IBM Research Laboratory (Zürich), 1995−1999.

(45) Troullier, N.; Martins, J. L. *Phys. Rev. B* **1991**, *43*, 1993.

(46) Kleinman, L.; Bylander, D. M. *Phys. Rev. Lett.* **1982**, *48*, 1425.

(47) Bühl, M. *J. Phys. Chem. A* **2002**, *106*, 10505.

(48) Åstrand, P.-O.; Ruud, K.; Sundholm, D. *Theor. Chem. Acc.* **2000**, *103*, 365.

(49) Dalton, a molecular electronic structure program, release 1.2. Helgaker, T.; Jensen, H. J. A.; Jørgenson, P.; Olsen, J.; Ruud, K.; Ågren, H.; Auer, A. A.; Bak, K. L.; Bakken, V.; Christiansen, O.; Coriani, S.; Dahle, P.; Dalskov, E. K.; Enevoldsen, T.; Fernandez, B.; Hättig, C.; Hald, K.; Halkier, A.; Heiberg, H.; Hettema, H.; Jonsson, D.; Kirpekar, S.; Kobayashi, R.; Koch, H.; Mikkelsen, K. V.; Norman, P.; Packer, M. J.; Pedersen, T. B.; Ruden, T. A.; Sanchez, A.; Saue, T.; Sauer, S. P. A.; Schimmelpfennig, B.; Sylvester-Hvid, K. O.; Taylor, P. R.; Vahtras, O. 2001.

(50) Bühl, M.; Imhof, P.; Repisky, M. *Chem. Phys. Chem.* **2004**, *5*, 410.

(51) Bühl, M.; Gaemers, S.; Elsevier: C. J. *Chem. Eur. J.* **2000**, *6*, 3272.

(52) Bühl, M. *Theor. Chem. Acc.* **2002**, *107*, 336.

(53) Bramley, R.; Brorson, M.; Sargeson, A. M.; Schäffer, C. E. *J. Am. Chem. Soc.* **1985**, *107*, 2780.

(54) Koch, W.; Holthausen, M. C. *A Chemist's Guide to Density Functional Theory;* Wiley-VCH: 2000.

(55) Quantum chemical zero-point corrections essentially preserve the symmetries of the equilibrium geometries.

(56) Isolated **6** is not stable in the gas phase, where it would ionize spontaneously. In the calculations with atom-centered Gaussian-type basis sets, it is the finite size of the latter that prevents electron detachment. In the plane-wave calculations, the same is achieved by the specific treatment of the electrostatic potentials under the cluster boundary conditions, where compensating background charges are involved. No artifacts pointing to such a spontaneous electron detachment are encountered in the CPMD calculations.

(57) Jameson, C. J.; Rehder, D.; Hoch, M. *J. Am. Chem. Soc.* **1987**, *109*, 2589.

(58) Minaev, B.; Vaara, J.; Ruud, K.; Ågren, H. *Phys. Lett.* **1998**, *295*, 455.

(59) Cromp, B.; Carrington, T.; Salahub, D. R.; Malkina, O. L.; Malkin, V. G. *J. Chem. Phys.* **1999**, *110*, 7153.

(60) A referee suggested to apply some empirical scaling to the metal−ligand bond distances before computing the chemical shifts. While such a procedure may be feasible for highly symmetrical complexes, we have not attempted to do this, because it is not clear how to implement it in a general, rigorous way without impeding the predictive power.

(61) Accurate computations of EFGs require large basis sets and sophisticated treatments of electron correlation and relativity, see e.g. Schwerdtfeger, P.; Pernpointer, M.; Nazarewicz, W. In *Calculation of NMR and EPR Parameters. Theory and Applications*; Kaupp, M., Bühl, M., Malkin, V. G., Eds.; Wiley-VCH: Weinheim, 2004; p 279.

(62) *The Principles of Nuclear Magnetism*; Abragam, A., Ed.; Oxford University Press: Oxford, 1961.

(63) *C-13-NMR Spectroskopie;* Kalinowski, H.-O., Berger, S., Braun, S., Eds.; Thieme: Stuttgart, 1984.

(64) Sumner, G. G.; Klug, H. P.; Alexander, L. E. *Acta Cyrstallogr.* **1964**, *17*, 732.

(65) Sweany, R. L.; Brown, T. L. *Inorg. Chem.* **1977**, *16*, 415.

(66) Kenny, J. P.; King, R. B.; Schaefer, H. F., III *Inorg. Chem.* **2001**, *40*, 900.

(67) Folga, E.; Ziegler, T. *J. Am. Chem. Soc.* **1993**, *115*, 5169.

(68) Bühl, M. In *Encyclopedia of Computational Chemistry*; Schleyer, v. R. P., Schreiner, P. R., Alhinger, N. L., Clark, T., Gasteiger, J., Kollman, P., III, H. F. S., Eds.; Wiley: 1996; p 1835.

(69) Gonzalez, C.; Schlegel, H. B. *J. Chem. Phys.* **1989**, *90*, 2154.

(70) Gonzalez, C.; Schlegel, H. B. *J. Phys. Chem.* **1990**, *94*, 5523.

(71) Mooberry, E. S.; Pupp, M.; Slater, J. L.; Sheline, R. K. *J. Chem. Phys.* **1971**, *55*, 3655.

(72) Stryer, L. *Biochemistry*, 4th ed.; Freemann: New York, 1995.

(73) Tavagnacco, C.; Balducci, G.; Costa, G.; Taschler, K.; von Philipsborn, W. *Helv. Chim. Acta* **1990**, *73*, 1469.

(74) Altman, L. J.; Laungani, D.; Gunnarsson, G.; Wennerström, H.; Forsén, S. *J. Am. Chem. Soc.* **1978**, *100*, 8264.

(75) Jordan, M. J. T.; Del Bene, J. E. *J. Am. Chem. Soc.* **2000**, *122*, 2101.

(76) Del Bene, J. E.; Jordan, M. J. T. *J. Phys. Chem. A* **2002**, *1−6*, 5385.

(77) McNeill, E. A.; Scholer, F. R. *J. Am. Chem. Soc.* **1977**, *99*, 6243.

(78) Klüfers, P. *Z. Kristallogr.* **1984**, *167*, 253.

(79) Xie, X.; Au-Yeung, S. C. F.; Liu, H. *J. Mol. Struct. (THEOCHEM)* **1995**, *331*, 181.

(80) Barclay, G. A.; Hoskins, B. F. *J. Chem. Soc.* **1962**, 586.

(81) Beatti, J. K.; Best, S. P. *Coord. Chem. Rev.* **1997**, *166*, 391.

(82) Lucken, E. A. C.; Noack, K.; Williams, D. F. *J. Chem. Soc. (A)* **1967**, p 148.

(83) Benn, R.; Cibura, K.; Hoffmann, P.; Jonas, K.; Rufinska, A. *Organometallics* **1985**, *4*, 2214.

(84) Spiess, H. W.; Haas, H.; Hartmann, H. *J. Chem. Phys.* **1969**, *50*, 3057.

(85) Juranić, N. *Inorg. Chem.* **1983**, *22*, 521.

(86) Juranić, N.; Ćelap, M. B.; Vučelić, D.; Malinar, M. M.; Radivojša, P. N. *Spectrochim. Acta* **1979**, *35A*, 997.

(87) Asaro, F.; Liguori, L.; Pellizer, G. *Phys. Chem. Chem. Phys.* **1999**, *1*, 4981.

(88) Leung, P. C.; Coppers, C. *Acta Crystallogr.* **1983**, *B39*, 535.

(89) The chemical shift was obtained by using the mean computed ^{13}C shielding of $Fe(CO)_5$ as a reference and the experimental chemical shift of the latter ($\delta = 211.0$)[63] for conversion.

CT049920O